J Mol Model (2012) 18:2483–2491
DOI 10.1007/s00894-011-1279-x

ORIGINAL PAPER

Substituent effects on geometric and electronic properties of iron tetraphenylporphyrin: a DFT investigation

Lu Wei · Yuanbin She · Yanmin Yu · Xiaoqian Yao · Suojiang Zhang

Received: 1 July 2011 / Accepted: 11 October 2011 / Published online: 28 October 2011

Abstract To investigate the effects of the substituents, substituent positions and axial chloride ligand on the geometric and electronic properties of the iron tetraphenylporphyrin (FeTPP), a series of the substituented iron tetraphenylporphyrins and their chlorides, FeT(*o/p*-R)PP and FeT(*o/p*-R)PPCl (R = −H, -Cl, -NO_2, -OH, -OCH_3), were systematically calculated without any symmetry constraint by using DFT method. For geometric structure, the substituent position and axial Cl ligand change the configuration of the iron porphyrin obviously. The *ortho*-substituents prefer making the phenyls perpendicular to the porphyrin ring; the axial chloride draws the central Fe ion ~0.500 Å out of the porphyrin plane toward the ligand. With regard to electronic properties, it is found that E_{LUMO} could be related to the catalytic activity. The electron-withdrawing group always lowers the energies of both frontier orbitals, while the electron-donating one heightens them simultaneously, but they affect the E_{HOMO} and E_{LUMO} in the same sequence, -NO_2 < −Cl < −H < −OH < −OCH_3. The substituent effects on the central Fe ion were explored by calculating NBO charge distribution, spin density and natural electron configuration.

Keywords DFT · Electronic properties · Geometric properties · Iron tetraphenylporphyrin · Substituent effect

Introduction

Metalloporphyrins, as one of the most promising organometallic complexes, have drawn lots of attention for several decades due to their biological significance and applications [1–3]. Inspired by cytochrome P450 enzymes, many researchers have explored the metalloporphyrin as a model compound to catalyze the oxidative hydroxylation of alkanes under mild conditions [4–11]. During the process of seeking the most effective metalloporphyrin catalyst, it has been revealed that the nature of the porphin macrocycle, the axial ligand, and the central metal ion can determine the catalytic characteristics of these complexes. In particular, it has been proved that the catalytic performance of metalloporphyrins can be successfully modulated with different substituents [12–15]. For example, some halogenated iron tetraphenylporphyrins (FeTPPs) are far more active as the catalysts than non-halogenated ones, and the catalytic activity is increased with the degree of halogenation [11]. Besides, other substituents can also be introduced into the iron tetraphenylporphyrin, promoting the performance of the complex as a catalyst. Wang et al. [16] developed a synthetic technology of *p*-nitrobenzoic acid with molecular oxygen by using metalloporphyrins M^{III}T(*o/p*-R)PPCl (R = −Cl, -OH, -NO_2, -CH_3, -OCH_3; M = Fe, Co, Mn) as biomimetic catalysts. The results show that the catalytic activities are dependent on the nature of the substituted groups and the central metal ions of metalloporphyrins. For the same center metal ions, the more powerful electron-withdrawing groups engender the higher catalytic activities of the metalloporphyrins. Liu et

Electronic supplementary material The online version of this article (doi:10.1007/s00894-011-1279-x) contains supplementary material, which is available to authorized users.

L. Wei · Y. She (✉) · Y. Yu
Institute of Green Chemistry and Fine Chemicals, Beijing University of Technology,
100124 Beijing, China
e-mail: sheyb@bjut.edu.cn

X. Yao · S. Zhang
State Key Laboratory of Multiphase Complex Systems,
Institute of Process Engineering, Chinese Academy of Sciences,
100190 Beijing, China

al. [17] used 15 iron (III) porphyrin compounds with different substituents and different axial ligands to catalyze cyclohexane hydroxylation under room temperature and atomsphere pressure, then chose it as a model reaction to perform quantitative structure-activity relationship (QSAR) studies. Meanwhile, the theoretical investigations on the substituented iron tetraphenylporphyrin have also been carried out. Lü et al. [18] performed the geometric structure optimization of iron tetraphenylporphyrin chloride, FeTPPCl, and a number of its halogenated complexes by PM3 semi-empirical quantum calculation. Liao et al. [19] employed a number of density functionals to investigate the electronic structures of some tetraphenyl-substituted, four-coordinate iron(II) porphyrins, including FeTPP, iron tetra(α, α, α, α-orthopivalamide)phenylporphyrin (FeTpivPP) and halogenated iron porphyrins ($FeTPPX_n$, X = F, Cl; n=20, 28).

Despite these research works, a systematical theoretical investigation on the rule of substituent effects is still rare to date, especially using density functional theory (DFT) method. Besides, it seems to remain uncertain with regard to the electronic nature of the substituent effects, e.g., how the substituents influence the interaction between the central metal ion and the porphyrin ring, which is critical for exploring the interaction between the catalyst and the substrate. So in this work, a comprehensive calculation for FeT(*o/p*-R)PP and FeT(*o/p*-R)PPCl (R = −H, -Cl, $-NO_2$, -OH, $-OCH_3$) (shown in Fig. 1) was carried out. Two typical electron-withdrawing substituents, -Cl and $-NO_2$, as well as two typical electron-donating ones, -OH and $-OCH_3$, were chosen as the representatives to investigate the effects of the various substituents, different substituent positions at the phenyl and axial chloride ligand on the geometric and electronic structure of FeTPP. The properties were extensively considered, including bond length, bond angle, dihedral angle, the energies of frontier orbitals, charge population, spin density and electronic configuration of central Fe ion. The information could provide a deeper sight into the substituent effects observed in the metalloporphyrin catalysis. It is hoped that the work would be instructive for the modulation and design of metalloporphyrin catalysts.

Computational methods

All calculations were carried out using Gaussian09 program package [20]. The hybrid Becke-Lee-Yang-Parr (B3LYP) functional [21, 22] and the 6-31 G(d) basis set were used for complete geometry optimization without any symmetry constraint. The level has been proved suitable for geometry optimization of iron porphyrins [23–29]. The following frequency analysis revealed that all the structures obtained in this work had no imaginary vibration, indicating that the lowest energy structures for all of the complexes were truly local minima in the potential energy surfaces. The natural electron configuration (NEC) was studied by natural bond orbital (NBO) analysis [30] using NBO module contained in Gaussian09 program on the basis of the minimized structures. According to our practice, it was found that there was a severe convergence problem during the calculation of iron porphyrins. Thus the quadratic convergence SCF method, termed "SCF = QC" in the Gaussian program, was employed. Although the algorithm was rather time-consuming, it was more reliable for reaching a convergence point and it appeared to be the only effective way to solve the problem in terms of the methods we had tried.

For iron porphyrins, it is well accepted that the spin multiplicity, M, has a substantial influence on their total energies. Usually, the structure with the lowest energy is thermodynamically reasonable, which is a prerequisite for the theoretical investigation. Thus FeT(*o/p*-R)PP with M= 1, 3, 5 and FeT(*o/p*-R)PPCl with M=2, 4, 6 were examined and the spin state with the lowest energy was obtained. The spin state with the lowest energy is the triplet for FeT(*o/p*-R)PP, whereas the sextet for FeT(*o/p*-R)PPCl. The results for FeT(*o/p*-R)PP confirm the previous experimental and

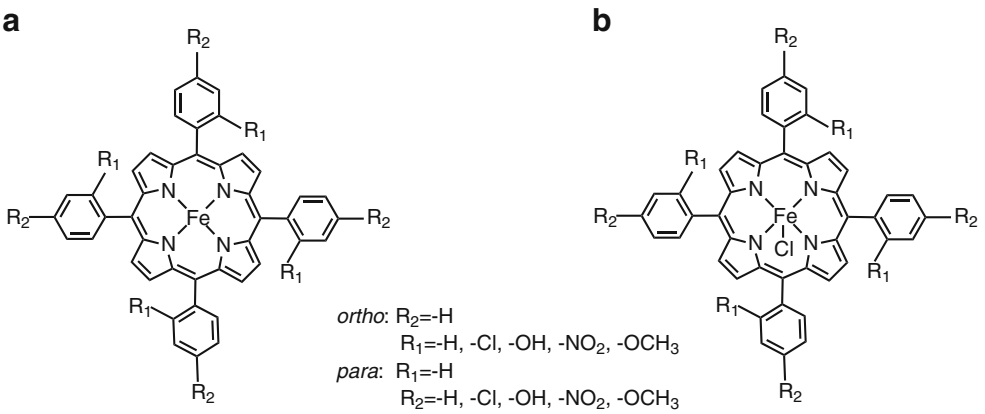

Fig. 1 The structures of (a) FeT(*o/p*-R)PP and (b) FeT(*o/p*-R)PPCl (R=−H, -Cl, $-NO_2$, -OH, $-OCH_3$)

theoretical studies [19, 31–39]. For FeT(*o/p*-R)PPCl, Scheidt and Reed [40] have pointed out that the coordination of strong or moderate field ligands usually results in low-spin state, while the coordination of weak field ligands is inclined to cause high-spin state. Since the chloride ligand could be considered as a weak field ligand [17], the results of FeT(*o/p*-R)PPCl in this work are reasonable and agree with earlier reports [1, 17, 41, 42]. In a word, the reasonable spin states have been predicted, which provides the evidence for the validity of the theoretical level we used. Only the spin states with the lowest energies were chosen for further discussion.

Results and discussion

Geometric properties

Despite no symmetry constraint, the optimized structures of FeT(*o/p*-R)PP and FeT(*o/p*-R)PPCl are still highly symmetrical, thus only average values of selected geometrical parameters are given, including bond lengths, bond angles and dihedral angles. The data about bond lengths are listed in Tables 1 and 2 (other geometrical parameters are given in Online resources 1–4). The atom notation is shown in Fig. 2.

As can be seen from Table 1, the calculated bond lengths of FeTPP, such as C_β-C_β, C_α-C_β, N-C_α and C_α-C_m, are 1.359 Å, 1.439 Å, 1.385 Å and 1.398 Å, respectively. They are in excellent agreement with earlier research works [33–35]. The Fe atom locates in the porphyrin plane. Fe-N bond length, 1.987 Å, is longer than the calculated value of 1.970 Å by Liao et al. [33, 34], the experimental data of 1.972 Å [35, 43] and 1.966 Å [32], which is probably caused by LYP correlation at B3LYP level [44]. Table 2 shows that for FeTPPCl, the Fe-N and Fe-Cl bond lengths are 2.088 Å and 2.237 Å, which are in agreement with the experimental values 2.060-2.078 Å and 2.211 Å [45]. The axial chloride ligand mainly influences the Fe-N bond length and distance of Fe atom out of the plane defined by four porphyrin nitrogen atoms, that is, the Fe-N bond is elongated by ~0.01 Å and the Fe atom is drawn 0.500 Å out of the plane toward the ligand, compared with the counterparts of FeTPP.

With regard to the effects of the various substituents and substitution positions at the phenyl, the differences caused by these factors are usually in the magnitude order of 10^{-3} Å for both FeT(*o/p*-R)PP and FeT(*o/p*-R)PPCl, indicating the bond lengths keep almost constant with the changes of the substituents and substitution positions at the phenyl.

Other geometric parameters, such as bond angles and dihedral angles (Online resources 1–4), also exhibit insensitivity to the substituents, substitution positions at the phenyl and the axial Cl ligand. The only exception is the dihedral angle of C_α-C_m-C_{ben1}-C_{ben2}. For both FeT(*o/p*-R)PP and FeT(*o/p*-R)PPCl, the C_α-C_m-C_{ben1}-C_{ben2} of iron porphyrins with *para*-substituented groups is in the range from 64° to 69°, while the phenyls with *ortho*-substituented groups prefer to be perpendicular to the plane of the porphyrin ring. It should be ascribed to more severely electronic and steric repulsions between the *ortho*-substituented group at the phenyl and the porphyrin ring. The results provide evidence for greater steric hindrance caused by *ortho*-substituents. The phenyls perpendicular to the plane of the porphyrin ring could make the self-aggregation harder. It is well accepted that the self-aggregation of metalloporphyrins could easily occur and bring about degradation of catalytic ability [16]. So in this sense, it is reasonable to infer that Fe porphyrins with *ortho*-substituents might exhibit better performance than those with *para*-substituents. The conclusion is in agreement with the experimental results [16].

Properties of frontier orbitals

According to the frontier molecular orbital theory, the frontier orbitals (HOMO and LUMO) of reactants can determine the way in which the molecule interacts with

Table 1 Selected bond lengths (in Å) of FeT(*o/p*-R)PP with M=3

FeT(*o/p*-R)PP	C_β-C_β	C_α-C_β	N-C_α	C_α-C_m	C_m-C_{ben1}	C_β-H	Fe-N	d[a]
FeTPP	1.359	1.439	1.385	1.398	1.495	1.080	1.987	0.000
FeT(*p*-Cl)PP	1.358	1.440	1.385	1.397	1.497	1.080	1.989	0.000
FeT(*p*-OH)PP	1.358	1.439	1.384	1.398	1.495	1.080	1.989	0.000
FeT(*p*-NO_2)PP	1.358	1.440	1.384	1.397	1.496	1.080	1.990	0.000
FeT(*p*-OCH_3)PP	1.359	1.439	1.385	1.398	1.495	1.080	1.987	0.000
FeT(*o*-Cl)PP	1.358	1.440	1.383	1.394	1.499	1.080	1.988	0.000
FeT(*o*-OH)PP	1.358	1.440	1.384	1.394	1.499	1.080	1.988	0.000
FeT(*o*-NO_2)PP	1.358	1.439	1.380	1.395	1.500	1.080	1.993	0.000
FeT(*o*-OCH_3)PP	1.358	1.440	1.383	1.395	1.500	1.080	1.989	0.000

[a]distance of Fe atom out of the plane defined by four porphyrin nitrogen atoms

Table 2 Selected bond lengths (in Å) of FeT(*o*/*p*-R)PPCl with M=6

FeT(*o*/*p*-R)PPCl	C_β-C_β	C_α-C_β	N-C_α	C_α-C_m	C_m-C_{ben1}	C_β-H	Fe-N	Fe-Cl	d
FeTPPCl	1.360	1.441	1.381	1.403	1.498	1.080	2.088	2.237	0.500
FeT(*p*-Cl)PPCl	1.360	1.441	1.380	1.403	1.497	1.080	2.088	2.234	0.500
FeT(*p*-OH)PPCl	1.361	1.441	1.381	1.404	1.495	1.080	2.088	2.238	0.501
FeT(*p*-NO_2)PPCl	1.360	1.442	1.380	1.403	1.497	1.080	2.089	2.228	0.499
FeT(*p*-OCH_3)PPCl	1.360	1.441	1.381	1.403	1.497	1.080	2.088	2.239	0.501
FeT(*o*-Cl)PPCl	1.360	1.442	1.379	1.400	1.500	1.080	2.087	2.231	0.503
FeT(*o*-OH)PPCl	1.360	1.441	1.380	1.401	1.500	1.080	2.087	2.238	0.505
FeT(*o*-NO_2)PPCl	1.360	1.441	1.378	1.400	1.501	1.081	2.088	2.223	0.506
FeT(*o*-OCH_3)PPCl	1.360	1.441	1.380	1.400	1.500	1.080	2.086	2.241	0.505

other species. Thus the properties of the frontier orbitals are critical for any chemical reaction. Koopmanns' theorem shows that the energy of the HOMO directly corresponds to the ionization potential (IP) and the energy of the LUMO has been used to estimate the electron affinity (EA), namely, $-E_{HOMO} \approx IP$ and $-E_{LUMO} \approx EA$ [31, 46]. Besides, the HOMO-LUMO gap (ΔE_{H-L}), equaling to the difference in energy between the HOMO and LUMO, is also a vital stability index [47]. A small HOMO-LUMO gap implies high chemical activity for the molecule in chemical reactions [48–52]. Tables 3 and 4 show the data for FeT(*o*/*p*-R)PP with M=3 and FeT(*o*/*p*-R)PPCl with M=6 (It should be noted that the data refer to alpha orbitals).

As shown in Tables 3 and 4, it can be found that the electron-withdrawing group, as a substituent at the phenyl or an axial ligand, always lowers both E_{HOMO} and E_{LUMO}, whereas the electron-donating one raises them simultaneously. Both the values of E_{HOMO} and E_{LUMO} are in the same sequence of - NO_2 < −Cl < −H < −OH < $-OCH_3$, which could be interpreted by the changes of the electron density of frontier orbitals caused by the substituent groups. The electron-withdrawing group may disperse the electron density in the porphyrin [17], making the electrons more delocalized in the π-conjugated electronic system of the porphyrin. As a result, the electronic repulsion is decreased, which lowers the energy levels of the frontier orbitals. The contrary effect might be found when the electron-donating group is introduced into FeTPP. With regard to the effect of substituent positions, *ortho*-substituents systematically make the energies of HOMO/LUMO higher than *para*-substituents. For the substituent locating at the phenyl *para*-position, the direct steric and electronic interactions between the *p*-substituents and the porphyrin core could be neglectable [53, 54]. But obviously, the electronic interaction between the *o*-substituents and the porphyrin ring is so powerful that the electron density in the π-conjugated electronic system of the porphyrin is increased, thus raising the energy levels of the frontier orbitals.

Earlier researches have pointed out that the catalytic activity of iron porphyrins is directly related to the Fe(III)/

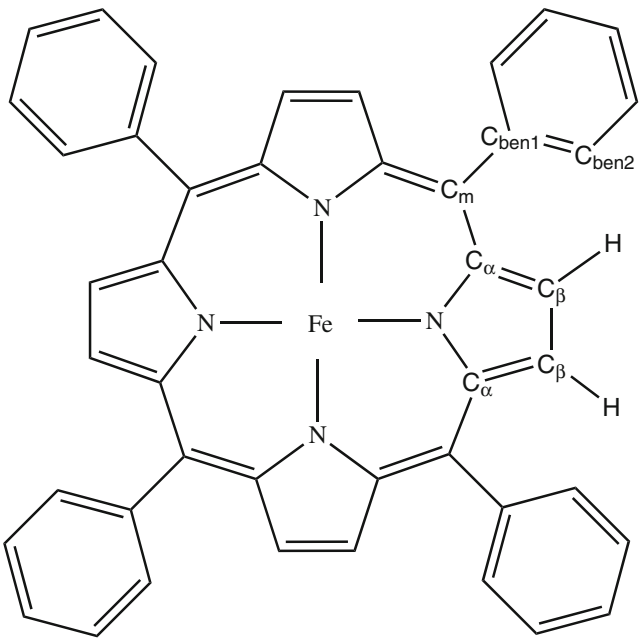

Fig. 2 Labeling diagram of the iron tetraphenylporphyrin

Table 3 E_{HOMO}, E_{LUMO} and HOMO-LUMO gap (in a.u.) of FeT(*o*/*p*-R)PP with M=3

FeT(*o*/*p*-R)PP	E_{HOMO}	E_{LUMO}	ΔE_{H-L}
FeTPP	−0.18346	−0.07526	0.10820
FeT(*p*-NO_2)PP	−0.21793	−0.11199	0.10594
FeT(*p*-Cl)PP	−0.19668	−0.08951	0.10717
FeT(*p*-OH)PP	−0.17951	−0.07324	0.10627
FeT(*p*-OCH_3)PP	−0.17465	−0.07155	0.10310
FeT(*o*-NO_2)PP	−0.19280	−0.08767	0.10513
FeT(*o*-Cl)PP	−0.19053	−0.08023	0.11030
FeT(*o*-OH)PP	−0.17504	−0.06523	0.10981
FeT(*o*-OCH_3)PP	−0.17390	−0.06349	0.11041

Table 4 E_{HOMO}, E_{LUMO} and HOMO-LUMO gap (in a.u.) of FeT(*o/p*-R)PPCl with M=6

FeT(*o/p*-R)PPCl	E_{HOMO}	E_{LUMO}	ΔE_{H-L}
FeTPPCl	−0.18823	−0.08764	0.10059
FeT(*p*-NO_2)PPCl	−0.22169	−0.12171	0.09998
FeT(*p*-Cl)PPCl	−0.20106	−0.10078	0.10028
FeT(*p*-OH)PPCl	−0.18198	−0.08464	0.09734
FeT(*p*-OCH_3)PPCl	−0.18110	−0.08191	0.09919
FeT(*o*-NO_2)PPCl	−0.19690	−0.09629	0.10061
FeT(*o*-Cl)PPCl	−0.19513	−0.09208	0.10305
FeT(*o*-OH)PPCl	−0.17960	−0.07580	0.10380
FeT(*o*-OCH_3)PPCl	−0.17914	−0.07489	0.10425

Fe(II) reduction potential of the porphyrin complex [11] and there is a positive linear correlation between the EAs of these species and their condensed-phase reduction potentials [14]. Taking $-E_{LUMO} \approx EA$ into account, the result of E_{LUMO} could be directly compared with the experiment. Virtually, the sequence of $-NO_2 < -Cl < -H < -OH < -OCH_3$ nearly reproduces the tendency of ref. [16]. It is mainly because the role of the LUMO in the biomimetic catalytic oxidation should be more important than the HOMO, since the oxidant, such as molecular oxygen, is activated by the coordination with the central metal ion. The LUMO of the iron porphyrin serves as an electron acceptor to accept the electron from the HOMO of the oxidant. The lower E_{LUMO} is favorable for lessening the energy gap between the LUMO of the iron porphyrin and the HOMO of the oxidant, making the electron density transfer between them more easily. Thus the catalytic activity is improved.

In addition, it could also be found by comparing the ΔE_{H-L} of Tables 3 and 4 that the axial chloride ligand systematically decreases the HOMO-LUMO gap, indicating that an axial electron-withdrawing group could indeed improve the chemical activity of FeTPP. The finding is positive for explaining the better catalytic performance of chloridized iron porphyrins observed in the experiments [11, 16, 17].

NBO charge distribution

The central Fe ion in the iron porphyrin is the active site in the catalysis, so its electronic properties are preconditions for deeply understanding the interaction between the catalyst and the substrate. Introducing different substituents in the porphin ring could change the properties of the iron ion, then give rise to a profound effect at a macroscopical level. Hence, NBO charge distribution, spin density and natural electron configuration of the central Fe ion were calculated to explore the substituent effects on the central metal ion.

Tables 5 and 6 list the NBO charges of Fe and N atoms. The charges of Fe atom in FeT(*o/p*-R)PP range from 1.030~1.190, whereas the counterparts in the iron porphyrin chlorides are about 1.44. The isolated iron ion usually carries +2 or +3 charge. But the calculated charges of Fe in FeT(*o/p*-R)PP and FeT(*o/p*-R)PPCl are much lower than these two valences, clearly indicating that the electron density has transferred from the porphyrin ligand to the iron ion.

Regarding the substituent effects on the charge, it is firstly noted that the axial chloride ligand exhibits remarkable electron-withdrawing and leveling effects (seen in Table 6). The charges of Fe in iron porphyrin chlorides are nearly 0.4 bigger than those in unligated iron porphyrins, while the differences originating from various substituents and different substituent positions are all in the order of 10^{-3}, revealing that the axial ligand totally covers other effects on the charge of Fe atom. Besides, due to Fe atom out of the porphyrin plane drawn by the axial ligand, the overlaps between iron and nitrogens in the porphyrin ring are decreased and the electron transfer from nitrogens to iron atom is handicapped, so there are more negative charges (~0.02) carried by nitrogens in the porphyrin ring. More static charges located at Fe and N atom enhance the Fe-N bonds in a form of the ionic bond.

Table 5 NBO charges of Fe and N atoms and the spin density of Fe in FeT(*o/p*-R)PP with M=3

FeT(*o/p*-R)PP	q_{Fe}	q_N	ρ_s (Fe)
FeTPP	1.177	−0.596/-0.617	2.171
FeT(*p*-NO_2)PP	1.184	−0.595/-0.615	2.172
FeT(*p*-Cl)PP	1.175	−0.597/-0.615	2.172
FeT(*p*-OH)PP	1.037	−0.598	1.997
FeT(*p*-OCH_3)PP	1.034	−0.597/-0.598	1.995
FeT(*o*-NO_2)PP	1.055	−0.592	1.997
FeT(*o*-Cl)PP	1.044	−0.595/-0.596/-0.597	1.995
FeT(*o*-OH)PP	1.038	−0.596/-0.597	1.996
FeT(*o*-OCH_3)PP	1.035	−0.597	1.996

Table 6 NBO charges of Fe and N atoms and the spin density of Fe in FeT(*o/p*-R)PPCl with M=6

FeT(*o/p*-R)PPCl	q_{Fe}	q_N	ρ_s (Fe)
FeTPPCl	1.444	−0.613/-0.614/-0.615	4.211
FeT(*p*-NO_2)PPCl	1.443	−0.612/-0.613	4.210
FeT(*p*-Cl)PPCl	1.444	−0.613/0.614	4.210
FeT(*p*-OH)PPCl	1.443	−0.613/-0.615	4.209
FeT(*p*-OCH_3)PPCl	1.444	−0.613/-0.615	4.210
FeT(*o*-NO_2)PPCl	1.440	−0.608	4.208
FeT(*o*-Cl)PPCl	1.444	−0.613/-0.614	4.212
FeT(*o*-OH)PPCl	1.445	−0.613/-0.614	4.213
FeT(*o*-OCH_3)PPCl	1.446	−0.614	4.213

Table 7 NEC of Fe atom in FeT(*o*/*p*-R)PP with M=3

FeT(*o*/*p*-R)PP	NEC	NEC of 3d orbital
FeTPP	$4s^{0.31}3d^{6.24}4p^{0.27}$	$(3d_{xy})^{1.800}(3d_{xz})^{1.935}(3d_{yz})^{1.020}(3d_{x2-y2})^{0.828}(3d_{z2})^{0.657}$
FeT(*p*-Cl)PP	$4s^{0.31}3d^{6.24}4p^{0.27}$	$(3d_{xy})^{1.845}(3d_{xz})^{1.945}(3d_{yz})^{1.010}(3d_{x2-y2})^{0.783}(3d_{z2})^{0.657}$
FeT(*p*-OH)PP	$4s^{0.47}3d^{6.24}4p^{0.27}$	$(3d_{xy})^{1.009}(3d_{xz})^{1.941}(3d_{yz})^{1.003}(3d_{x2-y2})^{1.473}(3d_{z2})^{0.809}$
FeT(*p*-NO_2)PP	$4s^{0.31}3d^{6.24}4p^{0.27}$	$(3d_{xy})^{1.796}(3d_{xz})^{1.934}(3d_{yz})^{1.021}(3d_{x2-y2})^{0.832}(3d_{z2})^{0.657}$
FeT(*p*-OCH_3)PP	$4s^{0.47}3d^{6.24}4p^{0.27}$	$(3d_{xy})^{1.037}(3d_{xz})^{1.927}(3d_{yz})^{1.018}(3d_{x2-y2})^{1.445}(3d_{z2})^{0.810}$
FeT(*o*-Cl)PP	$4s^{0.46}3d^{6.23}4p^{0.27}$	$(3d_{xy})^{1.001}(3d_{xz})^{1.945}(3d_{yz})^{0.997}(3d_{x2-y2})^{1.484}(3d_{z2})^{0.807}$
FeT(*o*-OH)PP	$4s^{0.47}3d^{6.23}4p^{0.27}$	$(3d_{xy})^{0.998}(3d_{xz})^{1.947}(3d_{yz})^{0.995}(3d_{x2-y2})^{1.486}(3d_{z2})^{0.808}$
FeT(*o*-NO_2)PP	$4s^{0.46}3d^{6.23}4p^{0.26}$	$(3d_{xy})^{0.995}(3d_{xz})^{1.948}(3d_{yz})^{0.995}(3d_{x2-y2})^{1.491}(3d_{z2})^{0.805}$
FeT(*o*-OCH_3)PP	$4s^{0.47}3d^{6.23}4p^{0.27}$	$(3d_{xy})^{0.995}(3d_{xz})^{1.948}(3d_{yz})^{0.996}(3d_{x2-y2})^{1.487}(3d_{z2})^{0.808}$

Regardless of the axial chloride ligand, it can be found from Table 5 that the substituent position also has an obvious effect on the charge of the central metal ion. The *o*-substituents systematically diminish ~0.01 positive charge of Fe ion in FeTPP, probably because the *o*-substituent is closer to the porphyrin ring than the *para* one. The electronic repulsion between the *o*-substituent and the porphyrin ring would make the ring more electron-riched, leading to an electron-donating effect for the charge of Fe ion. However, it is noteworthy that for *o*-substituents, the charges caused by electron-withdrawing groups are still more positive than those caused by electron-donating groups, indicating that electron-withdrawing groups have tried their best to disperse the electron density, although failing.

Lastly, the influence of various substituents is reflected by the data of FeT(*o*/*p*-R)PP with *p*-substituents. Without the complicated interaction between the substituent and the porphyrin ring [53, 54] nor the effect of the axial ligand, the charge of the central iron atom is in accord with the knowledge of the substituent, that is, the electron-withdrawing groups are apt to cause more positive charge than the electron-donating ones.

A more positive Fe charge means that the electron density around the central metal is dispersed, which is beneficial to the stabilization of LUMO, as well as the binding of iron porphyrins with the substrate [17]. According to the analysis of the frontier orbitals, the lower E_{LUMO} favors the higher catalytic activity. So the NBO charge of central metal ion could also reflect the effects of substituents on the catalytic activity.

Spin density

Although NBO charge distribution provides an obvious evidence for charge transfer, it cannot clarify what electrons are transferred. To explore the nature of the transferred electrons, the spin density, ρ_s, was introduced. The spin density is defined as the electron density of α electron minus the electron density of β electron. The distributions of the spin density on the central Fe ion are also contained in Tables 5 and 6. They are ~2.000 for unligated iron porphyrins with M=3 and ~4.200 for chlorine-ligated ones with M=6. The total spin density for the former is 2, whereas 5 for the latter.

The spin density of Fe atom in FeTPP is 2.171, bigger than the corresponding total spin density. According to the definition of the spin density, it could be analyzed that it is a net result of either α electron increasing or β electron decreasing. Considering the electron transfer from the ligand to the central metal ion, it is reasonable that the electrons with parallel spin (α electrons) are donated to the central metal ion. The earlier reports [36, 55] also found

Table 8 NEC of Fe atom in FeT(*o*/*p*-R)PPCl with M=6

FeT(*o*/*p*-R)PPCl	NEC	NEC of 3d orbital
FeTPPCl	$4s^{0.37}3d^{5.71}4p^{0.49}$	$(3d_{xy})^{1.104}(3d_{xz})^{1.000}(3d_{yz})^{1.100}(3d_{x2-y2})^{1.266}(3d_{z2})^{1.237}$
FeT(*p*-Cl)PPCl	$4s^{0.37}3d^{5.71}4p^{0.49}$	$(3d_{xy})^{1.111}(3d_{xz})^{1.000}(3d_{yz})^{1.102}(3d_{x2-y2})^{1.243}(3d_{z2})^{1.250}$
FeT(*p*-OH)PPCl	$4s^{0.37}3d^{5.71}4p^{0.49}$	$(3d_{xy})^{1.115}(3d_{xz})^{1.001}(3d_{yz})^{1.099}(3d_{x2-y2})^{1.238}(3d_{z2})^{1.255}$
FeT(*p*-NO_2)PPCl	$4s^{0.37}3d^{5.71}4p^{0.49}$	$(3d_{xy})^{1.111}(3d_{xz})^{1.000}(3d_{yz})^{1.104}(3d_{x2-y2})^{1.244}(3d_{z2})^{1.247}$
FeT(*p*-OCH_3)PPCl	$4s^{0.37}3d^{5.71}4p^{0.49}$	$(3d_{xy})^{1.103}(3d_{xz})^{1.000}(3d_{yz})^{1.102}(3d_{x2-y2})^{1.254}(3d_{z2})^{1.248}$
FeT(*o*-Cl)PPCl	$4s^{0.37}3d^{5.70}4p^{0.49}$	$(3d_{xy})^{1.106}(3d_{xz})^{0.999}(3d_{yz})^{1.104}(3d_{x2-y2})^{1.255}(3d_{z2})^{1.241}$
FeT(*o*-OH)PPCl	$4s^{0.37}3d^{5.70}4p^{0.49}$	$(3d_{xy})^{1.103}(3d_{xz})^{0.999}(3d_{yz})^{1.102}(3d_{x2-y2})^{1.260}(3d_{z2})^{1.240}$
FeT(*o*-NO_2)PPCl	$4s^{0.37}3d^{5.71}4p^{0.49}$	$(3d_{xy})^{1.108}(3d_{xz})^{0.999}(3d_{yz})^{1.107}(3d_{x2-y2})^{1.258}(3d_{z2})^{1.237}$
FeT(*o*-OCH_3)PPCl	$4s^{0.37}3d^{5.70}4p^{0.49}$	$(3d_{xy})^{1.102}(3d_{xz})^{0.999}(3d_{yz})^{1.101}(3d_{x2-y2})^{1.259}(3d_{z2})^{1.243}$

that there was an extensive π spin transfer in FeTPP, originating purely from the porphyrin-iron charge transfer.

In terms of the substituent effects for unligated iron porphyrins, it can be found that α electron transfer remains only in the cases of FeTPP with *p*-Cl and *p*-NO_2. The spin densities of Fe in the rest are 1.995∼1.997, slightly lower than the total spin density. But the nature of transferred electrons is totally different. Similar to the above analysis, it could be concluded that there must be the opposite spin electrons (β electrons) given to the central metal ion, despite slightness, that is to say, the electron-donating groups or *ortho*-substituents disperse the spin density located at the Fe atom, making its unpaired electrons reduced. It would affect the bonding with a substrate.

For FeT(*o/p*-R)PPCl, the effect of the axial ligand is predominant. The spin density of the axial Cl ligand is ranged from 0.25∼0.27. Considering the data listed in Table 6, there is still about 0.5 spin density distributed on the porphyrin ring. Compared with the unligated iron porphyrin, many more opposite spin electrons are transferred to the Fe atom from the porphyrin. They are favorable for electron pairing with the spin electrons of Fe atom, thus the axial chloride ligand might enhance the chemical interaction between the porphyrin ring and the central iron ion.

Natural electron configuration

To probe which orbitals are involved during charge transfer, the natural electron configuration of Fe atom is studied and the data are shown in Tables 7 and 8. It can be observed from Tables 7 and 8 that there are unneglectable populations on the 4 s and 4 p orbitals, showing that the iron ion performed an orbital hybridization of 3 d, 4 s and 4 p before bonding with the group orbitals of the porphyrin ligand.

For the unligated iron porphyrins, the population of 4 s orbital is obviously changed owing to the substituent effect, which is improved by the electron-donating groups or the *ortho*-substituents. Combined with the findings of the charge and the spin density of Fe atom, it could be concluded that the electron-donating groups or the *ortho*-substituents let more β electrons transfer to the 4 s orbital of the central Fe ion. It should be also noted that although the sum of the population of 3 d orbitals is the same, the population on each 3 d orbital has been changed. The electron-donating groups or the *ortho*-substituents deprive the electron density of $3d_{xy}$ and allocate it to $3d_{x2-y2}$ and $3d_{z2}$. For FeT(*o/p*-R)PPCl, the effect of the axial ligand is still predominant. The nearly identical natural electron configuration causes the almost unchanged central Fe atomic charge and spin density. The electrons are more evenly arranged on each 3 d orbital. The increment of the electronic population on $3d_{z2}$ should originate from the coordination interaction between Fe ($3d_{z2}$)-Cl ($3p_z$). These orbitals of FeT(*o/p*-R)PP and FeT(*o/p*-R)PPCl should be paid more attention when discussing different orbital interactions between the substituented iron porphyrins and the substrate.

Summary

A series of the substituted iron porphyrins, FeT(*o/p*-R)PP and FeT(*o/p*-R)PPCl (R = −H, -Cl, -OH, -NO_2, -OCH_3), were fully optimized without any symmetry constraint by using DFT method to systematically investigate the effects of the substituents, substituent positions and axial chloride ligand on both geometric and electronic properties.

For geometric structure, the substituent position and axial Cl ligand appear to be more powerful for changing the configuration of the iron porphyrin. The *ortho*-substituents are apt to make the phenyls perpendicular to the porphyrin ring; the axial chloride draws the central Fe atom ~0.500 Å out of the porphyrin plane toward the ligand.

For electronic properties, it is found that E_{LUMO} could be related to the catalytic activity by means of EA and Fe(III)/Fe(II) reduction potential. The rule of substituent effects on E_{LUMO} might provide a clue for seeking and designing the better metalloporphyrin catalyst. NBO charge distribution, spin density and NEC reveal that for unligated iron porphyrins, the electron-donating groups or the *ortho*-substituents let more β electrons transfer to the 4 s orbital of the central Fe ion and deprive the electron density of $3d_{xy}$ to $3d_{x2-y2}$ and $3d_{z2}$, while for their chlorides, the axial Cl ligand has a dominant effect so that the effects of other factors are totally covered. The results would help researchers understand different behaviors of FeT(*o/p*-R)PP and FeT(*o/p*-R)PPCl when interacting with the substrate, such as molecular oxygen.

It is hoped that this work could provide a deeper insight into the role the substituents play in metalloporphyrin modulation and is meaningful and instructive for both the experimental and theoretical studies of the metalloporphyrins, especially in the field of catalysis.

Acknowledgments This work was supported by the State Key Program of National Natural Science of China (Grant No. 21036009), the Funding Project for Academic Human Resources Development in Institutions of Higher Learning under the Jurisdiction of Beijing Municipality (Grant No.PHR201107104 and PHR200907105) and the National Natural Science Foundation of China for the Youth (Grant No. 20903007).

References

1. Asghari-Khiavi M, Safinejad F (2010) Theoretical studies on metal porphyrin halides: Geometrical parameters and nonlinear optical responses. J Mol Model 16:499–503

2. Grinstaff MW, Hill MG, Labinger JA, Gray HB (1994) Mechanism of catalytic oxygenation of akanes by halogenated iron porphyrins. Science 264:1311–1313
3. Dolphin D, Felton RH (1974) Biochemical significance of porphyrin pi cation radicals. Accounts Chem Res 7:26–32
4. Groves JT, McClusky GA (1976) Aliphatic hydroxylation via oxygen rebound - oxygen-transfer catalyzed by iron. J Am Chem Soc 98:859–861
5. Groves JT, Nemo TE, Myers RS (1979) Hydroxylation and epoxidation catalyzed by iron-porphine complexes - oxygen-transfer from iodosylbenzene. J Am Chem Soc 101:1032–1033
6. Groves JT, Kruper WJ, Nemo TE, Myers RS (1980) Hydroxylation and epoxidation reactions catalyzed by synthetic metalloporphyrinates - models related to the active oxygen species of cytochrome-P-450. J Mol Catal 7:169–177
7. Mansuy D, Bartoli JF, Chottard JC, Lange M (1980) Metalloporphyrin-catalyzed hydroxylation of cyclohexane by alkyl hydroperoxides - pronounced efficiency of iron-porphyrins. Angew Chem Int Edn 19:909–910
8. Groves JT, Nemo TE (1983) Aliphatic hydroxylation catalyzed by iron porphyrin complexes. J Am Chem Soc 105:6243–6248
9. Ji LN, Liu M, Hsieh AK, Hor TSA (1991) Metalloporphyrin-catalyzed hydroxylation of cyclohexane with molecular-oxygen. J Mol Catal 70:247–257
10. Meunier B (1992) Metalloporphyrins as versatile catalysts for oxidation reactions and oxidative DNA cleavage. Chem Rev 92:1411–1456
11. Lyons JE, Ellis PE, Myers HK (1995) Halogenated metalloporphyrin complexes as catalysts for selective reactions of acyclic alkanes with molecular-oxygen. J Catal 155:59–73
12. Yuan Y, Ji HB, Chen YX, Han Y, Song XF, She YB, Zhong RG (2004) Oxidation of cyclohexane to adipic acid using Fe-porphyrin as a biomimetic catalyst. Org Process Res Dev 8:418–420
13. Haber J, Matachowski L, Pamin K, Poltowicz J (2003) The effect of peripheral substituents in metalloporphyrins on their catalytic activity in Lyons system. J Mol Catal A-Chem 198:215–221
14. Chen HL, Ellis PE, Wijesekera T, Hagan TE, Groh SE, Lyons JE, Ridge DP (1994) Correlation between gas-phase electron-affinities, electrode-potentials, and catalytic activities of halogenated metalloporphyrins. J Am Chem Soc 116:1086–1089
15. Ellis PE, Lyons JE (1990) Selective air oxidation of light alkanes catalyzed by activated metalloporphyrins - the search for a suprabiotic system. Coord Chem Rev 105:181–193
16. Wang LH, She YB, Zhong RG, Ji HB, Zhang YH, Song XF (2006) A green process for oxidation of p-nitrotoluene catalyzed by metalloporphyrins under mild conditions. Org Process Res Dev 10:757–761
17. Liu N, Jiang GF, Guo CC, Tan Z (2009) Quantitative structure-activity relationship studies on ironporphyrin-catalyzed cyclohexane oxidation with PhIO. J Mol Catal A Chem 304:40–46
18. Lu QZ, Yu RQ, Shen GL (2003) The structure, catalytic activity and reaction mechanism modeling for halogenated iron-tetraphenylporphyrin complexes. J Mol Catal A Chem 198:9–22
19. Liao MS, Watts JD, Huang MJ (2007) Electronic structure of some substituted iron(II) porphyrins. Are they intermediate or high spin? J Phys Chem A 111:5927–5935
20. Frisch MJ et al. (2009) Gaussian 09, Revision A.02. Gaussian Inc Wallingford CT
21. Becke AD (1993) Density-functional thermochemistry.3. The role of exact exchange. J Chem Phys 98:5648–5652
22. Lee CT, Yang WT, Parr RG (1988) Development of the colle-salvetti correlation-energy formula into a functional of the electron-density. Phys Rev B 37:785–789
23. Lu X, Ma J, Sun R, Nan M, Meng F, Du J, Wang X, Shang H (2010) Substituent effects of iron porphyrins: Structural, kinetic, and theoretical studies. Electrochim Acta 56:251–256
24. Sicking W, Korth HG, Jansen G, de Groot H, Sustmann R (2007) Hydrogen peroxide decomposition by a non-heme iron(III) catalase mimic: A DFT study. Chem Eur J 13:4230–4245
25. Nakashima H, Hasegawa JY, Nakatsuji H (2006) On the reversible O_2 binding of the Fe-porphyrin complex. J Comput Chem 27:426–433
26. Nakashima H, Hasegawa JY, Nakatsuji H (2006) On the O_2 binding of Fe-porphyrin, Fe-porphycene, and Fe-corrphycene complexes. J Comput Chem 27:1363–1372
27. Kozlowski PM, Kuta J, Ohta T, Kitagawa T (2006) Resonance Raman enhancement of Fe^{IV}=O stretch in high-valent iron porphyrins: An insight from TD-DFT calculations. J Inorg Biochem 100:744–750
28. Charkin OP, Klimenko NM, Nguyen PT, Charkin DO, Mebel AM, Lin SH, Wang YS, Wei SC, Chang HC (2005) Fragmentation of heme and hemin(+) with sequential loss of carboxymethyl groups: A DFT and mass-spectrometry study. Chem Phys Lett 415:362–369
29. Ugalde JM, Dunietz B, Dreuw A, Head-Gordon M, Boyd RJ (2004) The spin dependence of the spatial size of Fe(II) and of the structure of Fe(II)-porphyrins. J Phys Chem A 108:4653–4657
30. Reed AE, Curtiss LA, Weinhold F (1988) Intermolecular interactions from a natural bond orbital, donor-acceptor viewpoint. Chem Rev 88:899–926
31. Feng XT, Yu JG, Liu RZ, Lei M, Fang WH, De Proft F, Liu SB (2010) Why iron? A spin-polarized conceptual density functional theory study on metal-binding specificity of porphyrin. J Phys Chem A 114:6342–6349
32. Hu CJ, Noll BC, Schulz CE, Scheidt WR (2007) Four-coordinate iron(II) porphyrinates: Electronic configuration change by intermolecular interaction. Inorg Chem 46:619–621
33. Liao MS, Scheiner S (2002) Electronic structure and bonding in metal porphyrins, metal = Fe, Co, Ni, Cu, Zn. J Chem Phys 117:205–219
34. Liao MS, Scheiner S (2002) Electronic structure and bonding in unligated and ligated FeII porphyrins. J Chem Phys 116:3635–3645
35. Collman JP, Hoard JL, Kim N, Lang G, Reed CA (1975) Synthesis, stereochemistry, and structure-related properties of alpha, beta, gamma, delta-tetraphenylporphinatoiron(II). J Am Chem Soc 97:2676–2681
36. Goff H, Lamar GN, Reed CA (1977) Nuclear magnetic-resonance investigation of magnetic and electronic properties of intermediate spin ferrous porphyrin complexes. J Am Chem Soc 99:3641–3646
37. Lang G, Spartalian K, Reed CA, Collman JP (1978) Mossbauer-effect study of magnetic-properties of S=1 ferrous tetraphenylporphyrin. J Chem Phys 69:5424–5427
38. Boyd PDW, Buckingham DA, McMeeking RF, Mitra S (1979) Paramagnetic anisotropy, average magnetic-susceptibility, and electronic-structure of intermediate-spin S=1 (5,10,15,20-tetraphenylporphyrin)iron(II). Inorg Chem 18:3585–3591
39. Mispelter J, Momenteau M, Lhoste JM (1980) Proton magnetic-resonance characterization of the intermediate (S=1) spin state of ferrous porphyrins. J Chem Phys 72:1003–1012
40. Scheidt WR, Reed CA (1981) Spin-state stereochemical relationships in iron porphyrins - implications for the hemoproteins. Chem Rev 81:543–555
41. Ghosh A, Persson BJ, Taylor PR (2003) *Ab initio* multiconfiguration reference perturbation theory calculations on the energetics of low-energy spin states of iron(III) porphyrins. J Biol Inorg Chem 8:507–511
42. Reed CA, Guiset F (1996) A "magnetochemical" series. Ligand field strengths of weakly binding anions deduced from S=3/2, 5/2 spin state mixing in iron(III) porphyrins. J Am Chem Soc 118:3281–3282
43. Tanaka K, Elkaim E, Li L, Jue ZN, Coppens P, Landrum J (1986) Electron-density studies of porphyrins and phthalocyanines.4.

Electron-density distribution in crystals of (meso-tetraphenylporphinato) iron(II). J Chem Phys 84:6969–6978
44. Rydberg P, Olsen L (2009) The accuracy of geometries for iron porphyrin complexes from density functional theory. J Phys Chem A 113:11949–11953
45. Scheidt WR, Finnegan MG (1989) Structure of monoclinic chloro (meso-tetraphenylporphyrinato)iron(III). Acta Crystallogr Sect C-Cryst Struct Commun 45:1214–1216
46. Zhan CG, Nichols JA, Dixon DA (2003) Ionization potential, electron affinity, electronegativity, hardness, and electron excitation energy: Molecular properties from density functional theory orbital energies. J Phys Chem A 107:4184–4195
47. Lewis D, Ioannides C, Parke D (1994) Interaction of a series of nitriles with the alcohol-inducible isoform of P450: Computer analysis of structure-activity relationships. Xenobiotica 24:401–408
48. Zhou Z, Parr RG (1990) Activation hardness: New index for describing the orientation of electrophilic aromatic substitution. J Am Chem Soc 112:5720–5724
49. Wei L, Yao X, Tian X, Cao M, Chen W, She Y, Zhang S (2011) A DFT investigation of the effects of doped Pb atoms on Pd_n clusters ($13 \leq n \leq 116$). Comput Theor Chem 966:375–382
50. Kalita B, Deka RC (2007) Stability of small Pd_n (n=1-7) clusters on the basis of structural and electronic properties: A density functional approach. J Chem Phys 127:244306
51. Gomes JRB, Lodziana Z, Illas F (2003) Adsorption of small palladium clusters on the relaxed alpha-Al2O3(0001) surface. J Phys Chem B 107:6411–6424
52. Nava P, Sierka M, Ahlrichs R (2003) Density functional study of palladium clusters. Phys Chem Chem Phys 5:3372–3381
53. Ikezaki A, Ikeue T, Nakamura M (2002) Electronic effects of *para*-substituents on the electron configuration of dicyano[meso-tetrakis(*p*-substituted phenyl)porphyrinato]iron(III) complexes. Inorg Chim Acta 335:91–99
54. Vangberg T, Ghosh A (1998) Direct porphyrin-aryl orbital overlaps in some *meso*-tetraarylporphyrins. J Am Chem Soc 120:6227–6230
55. Donohoe RJ, Atamian M, Bocian DF (1987) Characterization of singly reduced iron(II) porphyrins. J Am Chem Soc 109:5593–5599